Wavelength Selection and Growth of Görtler Vortices

Jerzy M. Floryan*
The University of Western Ontario, London, Canada
and
William S. Saric†
Virginia Polytechnic Institute and State University, Blacksburg, Virginia

An analysis of the growth of Görtler vortices and their effect on the laminar/turbulent transition process is presented. It is shown that only disturbances corresponding to the basic mode need to be considered and that the total growth of the disturbances depends upon the vortex size. Since the vortex wavelength is preserved in the streamwise direction, the vortex wavelength selection mechanism indirectly affects the total growth of the disturbances that dominate the instability process. It is shown that under ideal flow conditions, a vortex wavelength selection mechanism may be based on the maximum total growth of the disturbances. It is demonstrated that departures from the ideal flow conditions affect the vortex wavelength selection mechanism and the total growth of the vortices. The case of streamwise vorticity in the basic flow is analyzed and is shown to affect disturbances through a resonance.

Nomenclature

A = A^*/A_0^*, ratio of disturbance amplitude to the amplitude at the neutral point
D = streamwise extent of curved wall
G = $\hat{\epsilon}_c/\epsilon_v = R(\delta_r/\Re)^{1/2}$, Görtler number
h = $h_\phi = h_\psi$, metric coefficients for inviscid streamlines
$\Re$ = radius of curvature of wall
R = $U_\infty \delta_r/\nu = (U_\infty \tilde{\phi}/\nu)^{1/2}$, Reynolds number
U, V = dimensionless basic state velocities
U_∞ = freestream velocity, reference velocity
α = dimensionless wavenumber
β = dimensionless spatial amplification rate
$\hat{\beta}$ = β/G
β_0 = amplification rate for ideal flow conditions
β_1 = amplification rate correction due to mean-flow vorticity, Eqs. (21) and (39)
γ = mean-flow vortex spanwise wavenumber
δ_r = $(\nu\tilde{\phi}/U_\infty)^{1/2}$, boundary-layer reference length
ϵ_v = $1/R$, small viscous parameter
ϵ_c = $D/\Re$, small curvature parameter
$\hat{\epsilon}_c$ = $(\delta_r/\Re)^{1/2}$, small curvature parameter
ϵ_p = amplitude of Görtler vortices
ϵ_s = amplitude of mean-flow vortices
Λ = $(U_\infty \lambda/\nu)(\lambda/\Re)^{1/2}$, dimensionless wavelength parameter
λ = dimensional vortex wavelength
ν = kinematic viscosity
σ = amplification rate of mean-flow vorticity, Eq. (42)
ϕ = potential lines for chordwise coordinate
$\tilde{\phi}$ = dimensional chordwise distance from leading edge
ϕ_1 = $\epsilon_v \phi$, slow viscous scale
ϕ_2 = $\hat{\epsilon}_c \phi$, slow curvature scale
ψ = streamlines for normal-to-the-wall coordinate
ψ_2 = $\hat{\epsilon}_c \psi$, slow curvature scale

Presented as Paper 80-1376 at the AIAA 13th Fluid and Plasma Dynamics Conference, Snowmass, Colo., July 14-16, 1980; received Sept. 2, 1982; revision received Dec. 6, 1983.

*Assistant Professor, Faculty of Engineering Science. Member AIAA.

†Professor, Engineering Science and Mechanics Department. Associate Fellow AIAA.

I. Introduction

It is known that a boundary layer over a concave surface has a strong inviscid instability mechanism due to the presence of centrifugal forces. This mechanism may produce a secondary flow in the form of counterrotating vortices with axes parallel to the direction of the mean flow. Such a phenomenon is commonly referred to as the Görtler instability. The resulting streamwise vorticity has been known to be a strong modulator of transition to turbulence. Many experimental and analytical efforts have been aimed at the determination of conditions under which this unstable motion sets in and the form it assumes. Floryan and Saric[1] reviewed these efforts and determined the minimum critical Görtler number to be $G=0.4638$; however, they found no critical wavenumber α nor critical wavelength parameter Λ. The characteristics of the vortices generated by the instability are, therefore, determined by the disturbance growth process. The determination of the critical wavenumber may still be possible and may require the inclusion of higher order curvature and nonparallel effects.

The usual experimental technique for identifying the disturbances is to look for the spanwise periodic variations in the basic flow that are then interpreted as having been produced by the counterrotating vortex pairs. This is an indirect technique where the modulation of the basic state by the unstable motion is observed. Obviously, the unstable motion has to be sufficiently strong to permit such an identification and disturbances under neutral conditions may not necessarily fit into this category. The modulation of the mean flow will be observable only at a certain distance downstream from the neutral point. Thus, observations of the naturally occurring vortices[2-4] are very difficult and may not be well suited for measurements of the critical Görtler number. These experiments, however, provide valuable information about the form of the unstable motion. The distribution of disturbance velocity across the boundary layer is of particular interest. Disturbance velocity fields measured by Tani[2] and Bippes[4] suggest that the disturbances have the form of a single layer of vortices. This question will be discussed in Sec. III with particular attention paid to the higher modes.

The available measurements[2-4] point toward the difficulty of defining the spanwise wavenumber of the vortex emerging from the instability motion for the given geometry of the wall $\Re$ and flow conditions U_∞, ν. Tani[2] and Tani and Sakagami[3] performed a classical stability experiment in which they attempted to create as perfect a mean flow as possible and then

to observe the naturally occurring vortices. They concluded that they were unable to free themselves from the influence of the environment and thus the observed spanwise wavelength depended on the particular properties of the experimental apparatus and its flowfield. Bippes[4] confirmed their observations by noting that the disturbances in the oncoming stream had a very strong effect on the size of the observed vortices. In order to overcome the randomness of the background disturbances, Bippes[4] conducted experiments with screens that produced an isotropic field of disturbances in the oncoming flow. Then he observed that the naturally occurring vortices were those with the highest amplification rates, according to linear theory.[1] In all of these experimental observations it was noted that the vortex structure, once established, was preserved downstream. This fact makes the wavelength selection mechanism very important. Vortices of different wavelengths are amplified at different rates and reach different total growth and, therefore, have a different effect on transition. The question of a wavelength selection mechanism will be discussed in Sec. IV.

There is a dearth of analytical as well as experimental data concerning the streamwise growth of Görtler vortices and their effect on transition. Liepmann[5,6] observed the flow over a wall of constant curvature and found that the Görtler parameter had to reach a certain critical value before transition took place. Among other things, this value depended on the level of turbulence in the oncoming flow. Liepmann[5,6] determined the transition Görtler number to be $G=16.6$ for the lowest level of turbulence in his particular wind tunnel. According to Wortmann[7-9] and Bippes,[4] different types of instabilities follow the onset of the centrifugal instability, but precede the bursts of turbulence. The exact sequence of events depends, of course, on the flow configuration. Smith[10] computed the total streamwise growth of the vortices and found that their amplitude had to grow to a value of $A^*/A_0^* = \exp(10)$ in order to correlate the transition location found by Liepmann.[5,6] The analysis of the growth and total amplification of Görtler vortices based on the rational analysis of Görtler instability presented by Floryan and Saric[1] is discussed in Sec. IV.

The existing theoretical analyses of Görtler stability deal with the ideal flow conditions. Here the ideal flow conditions imply a purely two-dimensional basic flow. Such conditions are difficult to achieve experimentally. The possible deviations are due to the presence of the streamwise vorticity in the mean flow and due to spanwise waviness of the wall. The reader should note that spanwise waviness of the wall will create a spanwise periodic component in the mean flow that may be represented analytically in the same form as the streamwise vorticity. The available experimental data[2-4] suggest that the wavelength selection mechanism and growth of the vortices are very receptive to small departures from the ideal flow conditions. The questions of the influence of streamwise vorticity in the oncoming flow on the growth of Görtler vortices is addressed in Sec. V.

II. Problem Formulation

The unstable motion is driven by the local centrifugal forces and thus the evaluation of these forces is important for this analysis. The problem is, in general, configuration dependent since the local streamline curvature depends on the overall flowfield curvature rather than on the local value of the curvature of the wall. Here we follow the analysis of Floryan and Saric[1] and limit ourselves to linear stability theory. The configuration is chosen to be a cylinder with the streamwise cross section in the form of a circular arc; thus the wall that is modeled has a constant curvature $1/\Re$ over a finite streamwise extent D. Such a configuration possesses all of the characteristic geometric properties that are important for the intended analysis. The appropriate sketch of the flow situation is given in Fig. 1. The following presentation is limited to a short outline.

The analysis begins with the solution of the inviscid flow in the assumed configuration. A set of conformal transformations based on the Joukowski function provides an explicit expression for the stream and potential lines of the inviscid flow, thus allowing evaluation of the metric coefficients for the system of coordinates based on the inviscid streamlines and their orthogonals. For the boundary-layer type of analysis, expansions of the metric coefficients for the region close to the wall are needed. The terms that are required for further analysis are given as

$$h_\psi = h_\phi = 1 + 0(\epsilon_c), \qquad \frac{\partial h}{\partial \psi} = \epsilon_c \tag{1}$$

where ψ and ϕ are constants denoting the stream and potential lines, h_ψ and h_ϕ are the metric coefficients in the $d\psi$ and $d\phi$ directions, and $\epsilon_c = D/\Re$ is the dimensionless radius of curvature of the wall.

The basic state is chosen to be an incompressible, constant-property, two-dimensional flow. The Navier-Stokes equations are expressed in terms of a curvilinear orthogonal system of coordinates (ϕ,ψ,z), where z is the spanwise direction. The effects of viscosity are represented by the small parameter $\epsilon_v = \nu/U_\infty \delta_r$, while the effects of curvature are represented by the small parameter ϵ_c. The leading-order approximation in terms of ϵ_v and ϵ_c, when ϵ_v and ϵ_c are of the same order, results in the familiar boundary-layer equations for flow over a flat plate.

The stability analysis begins with the field equations made dimensionless by using δ_r as a length scale for the ψ and z coordinates, the freestream velocity U_∞ as a scale for the U, V, and u' velocities, a "viscous velocity" scale ν/δ_r for the v' and w' velocities, and $\rho\nu^2/\delta_r^2$ as a scale for the pressure disturbances. Here, U and V denote the streamwise and normal-to-the-wall mean-flow velocity components, while u', v', and w' stand for the streamwise, normal-to-the-wall, and spanwise disturbance-velocity components, respectively. Three-dimensional, steady, spatially growing disturbances are superposed on the mean flow as

$$\begin{aligned} u/U_\infty &= U(\phi,\psi) + u'(\phi,\psi,z) \\ v/U_\infty &= V(\phi,\psi) + (\nu/\delta_r U_\infty)\, v'(\phi,\psi,z) \\ w/U_\infty &= (\nu/\delta_r U_\infty)\, w'(\phi,\psi,z) \\ p/\rho U_\infty^2 &= P(\phi,\psi) + (\nu^2/\delta_r^2 U_\infty^2)\, p'(\phi,\psi,z) \end{aligned} \tag{2}$$

Floryan and Saric[1] showed first that this is the correct scaling for the Görtler vortex problem and that it leads to a set of equations with only a single stability parameter. The quantities in Eq. (2) are substituted into the field equations, the basic-state solution is applied to delete the basic-state terms, and the equations are linearized.

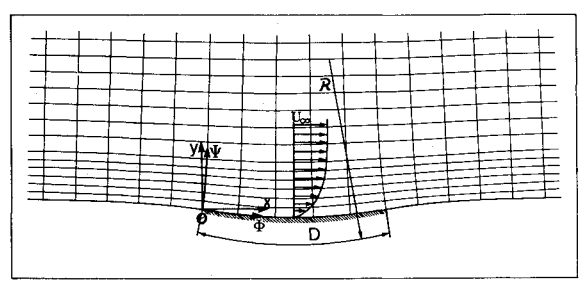

Fig. 1 Schematic diagram of the flow situation.

The dominating length scale of the problem δ_r is related to the boundary-layer thickness. Although the metric coefficient given by Eq. (1) is cast in terms of the streamwise extent of the curved wall D as a length scale, it is convenient to redefine it in terms of the length scale δ_r. Then the curvature parameter ϵ_c may be replaced by $\hat{\epsilon}_c=\sqrt{\delta_r/\Re}$. These parameters are not equal. However, they are of the same order of magnitude and one does not need to make a distinction between them on the intended level of approximation.[1] The metric coefficient assumes the form

$$h=1+0(\hat{\epsilon}_c), \qquad \frac{\partial h}{\partial \psi_2}=-\hat{\epsilon}_c^2 \tag{3}$$

where the slow scale $\psi_2=\hat{\epsilon}_c\psi$ is introduced to accommodate the rescaling of the coefficient.

Boundary-layer theory gives the chordwise variation of the mean flow in terms of the slow scale $\phi_1=\epsilon_v\phi$ (see Ref. 1). Definition of a proper scale governing the streamwise variation of the disturbance motion is more involved. The two small parameters, ϵ_v and $\hat{\epsilon}_c$, appearing in the stability problem, are assumed to be of the same order of magnitude. We may define two slow scales, $\phi_1=\epsilon_v\phi$ and $\phi_2=\hat{\epsilon}_c\phi$, and each of them is equally well suited for the analysis. One may argue that when viscous diffusion dominates, the unstable motion would depend on the same scale as the mean flow. On the other hand, if curvature effects are dominant, the proper scale would be ϕ_2. The distinction is only superficial and here we follow Floryan and Saric[1] and adopt the scale ϕ_1; however, we will come back to this question in Sec. IV.

The leading-order approximation for the disturbance equations results in the following set of equations:

$$T_1(U,V,u',v',w',p')=u'\frac{\partial U}{\partial \phi_1}+U\frac{\partial u'}{\partial \phi_1}+v'\frac{\partial U}{\partial \psi}+V\frac{\partial u'}{\partial \psi}-\frac{\partial^2 u'}{\partial \psi^2}-\frac{\partial^2 u'}{\partial z^2}=0 \tag{4}$$

$$T_2(U,V,u',v',w',p')=U\frac{\partial v'}{\partial \phi_1}+u'\frac{\partial V}{\partial \phi_1}+v'\frac{\partial V}{\partial \psi}+V\frac{\partial v'}{\partial \psi}+2G^2Uu'+\frac{\partial p'}{\partial \psi}-\frac{\partial^2 v'}{\partial \psi^2}-\frac{\partial^2 w'}{\partial z^2}=0 \tag{5}$$

$$T_3(U,V,u',v',w',p')=U\frac{\partial w'}{\partial \phi_1}+V\frac{\partial w'}{\partial \psi}+\frac{\partial p'}{\partial z}-\frac{\partial^2 w'}{\partial \psi^2}-\frac{\partial^2 w'}{\partial z^2}=0 \tag{6}$$

$$T_4(U,V,u',v',w',p')=\frac{\partial u'}{\partial \phi_1}+\frac{\partial v'}{\partial \psi}+\frac{\partial w'}{\partial z}=0 \tag{7}$$

The Görtler number G is defined as $G=(U_\infty\delta_r/\nu)\times\sqrt{\delta_r/\Re}$. Note that $\hat{\epsilon}_c$ does not appear explicitly in the equations and to this order of approximation the equations are configuration independent. This is a result of the correct scaling chosen in Eq. (2). The disturbances are assumed in the form of

$$(u',v',p')=[u(\psi),v(\psi),p(\psi)]\cos(\alpha z)\exp(\int\beta d\phi_1)$$
$$w'=w(\psi)\sin(\alpha z)\exp(\int\beta d\phi_1) \tag{8}$$

where α is the spanwise wavenumber and β the spatial amplification rate in the streamwise direction. Equations (4-8) are supplemented by the homogeneous boundary conditions expressing the no-slip and no-penetration conditions at the wall and the attenuation of disturbances far from the wall. The system of Eqs. (3-8) forms an eigenvalue problem for (α,β,G), which is solved with the numerical procedure described in Ref. 1.

III. The Unstable Motion

The Görtler number G is the critical stability parameter and when the curvature of the wall $(1/\Re)$, the velocity of the oncoming stream U_∞, and the type of the fluid ν are fixed, it may be interpreted as a measure of the distance from the leading edge. The increase of the Görtler number corresponds to moving downstream to a new location. Note that the length scale δ_r is a function of the streamwise location. Since the dimensionless wavenumber α is normalized with δ_r, it is a variable in the flow direction. It is convenient, therefore, to introduce a dimensionless wavelength parameter Λ, which is constant in the flow direction. Thus

$$\Lambda=\frac{U_\infty\lambda}{\nu}(\lambda/\Re)^{1/2} \tag{9}$$

where λ is the dimensional wavelength in the z direction.

Once the critical value of the Görtler number is reached, the unstable motion sets in. According to the experimental observations,[2-4] this motion has the form of one layer of counterrotating vortices. Thus, the disturbance velocity field corresponds to the first mode of the system of Eqs. (4-8). Herbert[11] pointed out that the observed disturbances may be produced by a superposition of the fundamental and higher modes. The neutral curves for the fundamental and higher modes are given in Fig. 2 and the associated disturbance velocity field is illustrated in Fig. 3. Note that zeroes of the w velocity profiles define centers of the vortices, while zeroes of the v velocity profiles define borders between different vertical layers of vortices. The eigenfunctions have been scaled by imposing the condition that $\max|u|=1$. The first mode corresponds to one layer of vortices, while the second and the third correspond to two and three layers of vortices, respectively. Note that the first mode is the most unstable and under normal circumstances it would dominate the instability process. The higher modes are relatively more stable due to the higher dissipation associated with the larger velocity gradients of the respective velocity fields. These modes would never appear under normal circumstances. However, under special conditions, i.e., vorticity present in the oncoming flow, they might be forced into the boundary layer. Moreover, Fig. 2 illustrates that care must be taken in calculations for $\alpha>1$ where the eigenvalue search may easily hit upon a higher mode. Since we are interested mostly in standard conditions, we will limit the further discussion to the fundamental mode.

The basic stability diagrams are given in Figs. 4 and 5. For convenience, we use the growth rate $\hat{\beta}=\beta/G$. The choice of the definition is justified in Sec. IV. The growth rate curves in terms of β are given in Ref. 1. Figure 4 is the standard stability diagram, while Fig. 5 is cast in terms of the wavelength parameter Λ defined in Eq. (9). The interpretation of both diagrams is straightforward if we consider the Görtler number to be a measure of the downstream distance from the leading edge. We begin in a streamwise location corresponding to, say, $G=0.3$. This is a stable region and all disturbances are damped out. When we move downstream and cross the location corresponding to the neutral curve, a whole band of wavelengths begins to grow. This band is unbounded on the side of small wavenumbers (large wavelength parameters). However, there is a well-defined boundary separating stable and unstable vortices on the side of large wavenumbers (small wavelength parameters). The cutoff wavelength parameter,

defining the lower bound of the unstable wavelengths, is $\Lambda_c = 44.29$. When vortices of decreasing size (increasing wavenumbers) are considered, the gradients of the associated disturbance velocity fields increase, leading to a higher dissipation. This dissipation is responsible for the elimination of the large wavenumber (small wavelength parameter) vortices.

When we cross the neutral curve moving toward increasing Görtler numbers, the question arises as to which wavenumber from the band of wavenumbers that becomes unstable will emerge as a result of the instability. Since there is no critical wavenumber nor critical wavelength parameter, the wavelength selection mechanism is determined by the disturbance growth process. We will come back to this question in Sec. IV.

In all of the experimental observations, it was noted that the wavelength of the disturbances was conserved in the flow direction. We may analyze the streamwise development of vortices of a particular wavelength by following lines of constant wavelength parameter Λ in Figs. 4 and 5. We choose a vortex corresponding to $\Lambda = 210$ for this purpose. It will be shown in Sec. IV that this is the most amplified and therefore the most dangerous disturbance. The appropriate disturbance velocity field at four streamwise locations is illustrated in Fig.

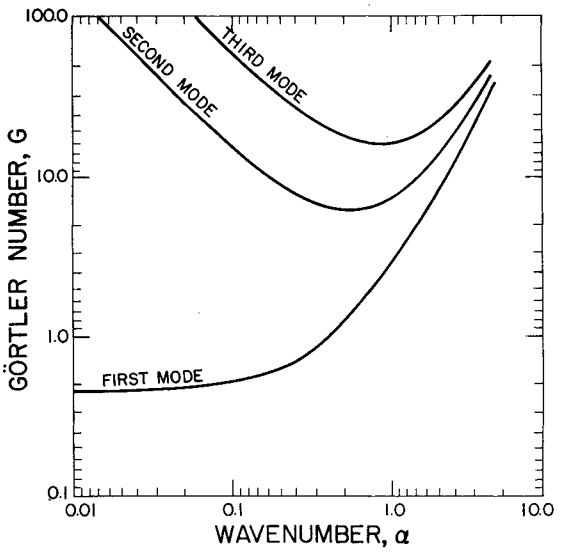

Fig. 2 Neutral stability curves for the first three modes of the Görtler instability of the Blasius boundary layer.

6. The eigenfunctions have been scaled by imposing the condition $\max(u) = 1$. At the neutral curve the distribution of the u velocity component is very similar to the mean flow. The v and w velocity components are relatively small. This suggests that the disturbances will be very difficult to identify at the very initial stages of the unstable motion. The developing spanwise periodicity of the mean flow seems to be the easiest identifiable sign of the developing unstable motion. As we move in the downstream direction (increasing G), the center of the vortex moves toward the wall and at the same time the magnitudes of the v and w velocity components increase considerably. The calculations show that disturbance velocity profiles for $\Lambda > 160$ ($\alpha < 0.15$) have the form similar to the mean velocity profile. For $\Lambda < 160$, the form is not like the mean flow; however, the corresponding vortices have never been observed to occur naturally.

The results of the experimental measurements of the disturbance velocity field are given in Refs. 2 and 4. Tani[2] investigated naturally occurring disturbances with the help of a hot wire. He measured only the u velocity component and his results agree well with the computed eigenfunction. Bippes[4] measured all three velocity components. His experiments were made using the hydrogen-bubble flow visualization technique. The velocity field was obtained by measuring the displacements of the hydrogen bubbles. The disturbances were triggered by the heated wires longitudinally placed close to the leading edge. Figure 7 gives the comparison of the measured disturbance velocity components with the appropriate eigenfunctions. The u, v, and w velocities are normalized with the maximum value of the u component, u_{max}. The ratios v_{max}/u_{max} and w_{max}/u_{max} found in the theory are approximately half the values found in the experiments. The relative numbers are 0.16 and 0.085 for the experiments and 0.08 and 0.04 for the theory. The difference is large; however, the measurements were made for very strong disturbances where, for example, the u component of the disturbance velocity was in the range of 10% of the mean flow. Nonlinear effects may be important under such conditions and this may explain the difference between experimental and theoretical data. Bippes'[4] experiments provide the only available measurements of the v and w disturbance velocity components. The only other statement about them is due to Wortmann,[8] who found that they are 20-30 times smaller than the u component.

IV. Wavelength Selection Mechanism and Growth of Vortices

The lack of a finite critical wavenumber α and a finite critical wavelength parameter Λ (Figs. 4 and 5) suggests that the wavelength selection mechanism is determined by the

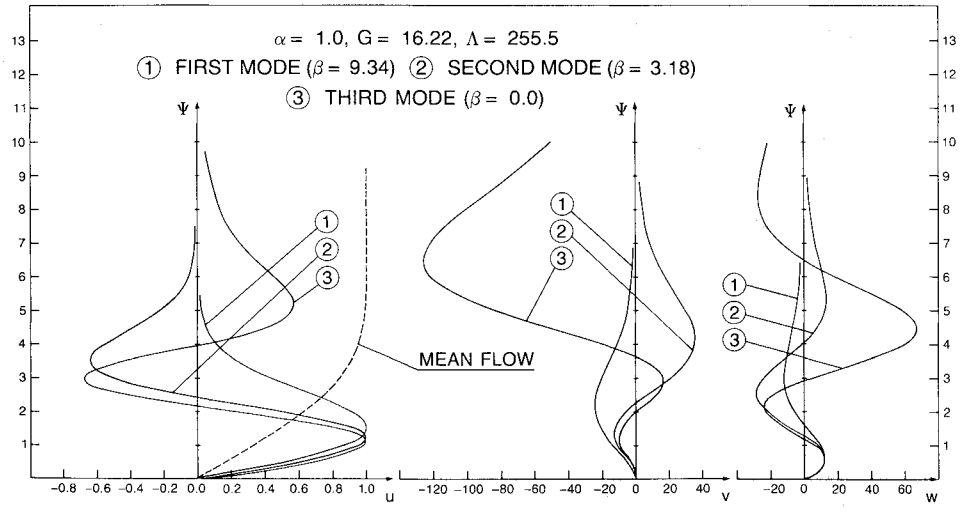

Fig. 3 The disturbance velocity field corresponding to the first three instability modes for the same wavelength parameter Λ and the same Görtler number G.

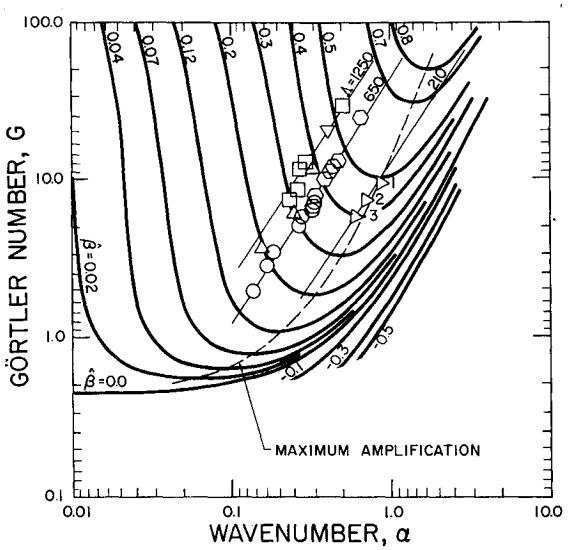

Fig. 4 Curves of constant amplification rate $\tilde{\beta}=\beta/G$ as a function of Görtler number G and wavenumber α for the Blasius boundary layer, comparison of theory with experiments. Experimental points due to Tani[2] and Tani and Sakagami[3]: ○ $U_\infty=11$ m/s, $\Re=10$ m; □ $U_\infty=7$ m/s, $\Re=5$ m; $U_\infty=7$ m/s, $\Re=3$ m; △ $U_\infty=16$ m/s, $\Re=10$ m; ▽ $U_\infty=7$ m/s, $\Re=1$ m. Experimental points due to Bippes[4]: ▷1 $U_\infty=0.3$ m/s, $\Re=0.5$ m; ▷2 $U_\infty=0.075$ m/s, $\Re=0.4$ m; ▷3 $U_\infty=0.075$ m/s, $\Re=1.0$ m (obtained with screens used to produce an isotropic field of disturbances in the oncoming flow).

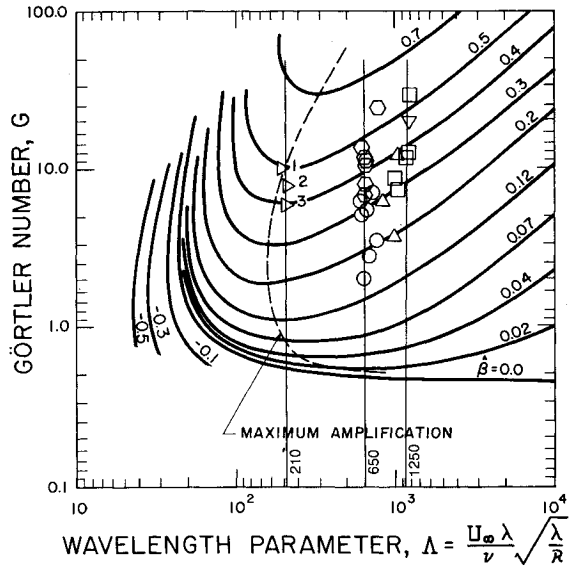

Fig. 5 Curves of constant amplification rate $\tilde{\beta}=\beta/G$ as a function of Görtler number G and the wavelength parameter Λ for the Blasius boundary layer (see Fig. 4 for legend).

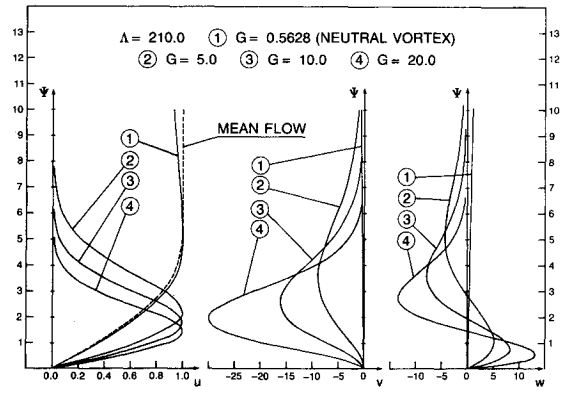

Fig. 6 Disturbance velocity field for the wavelength parameter $\Lambda=210$ as a function of Görtler number G.

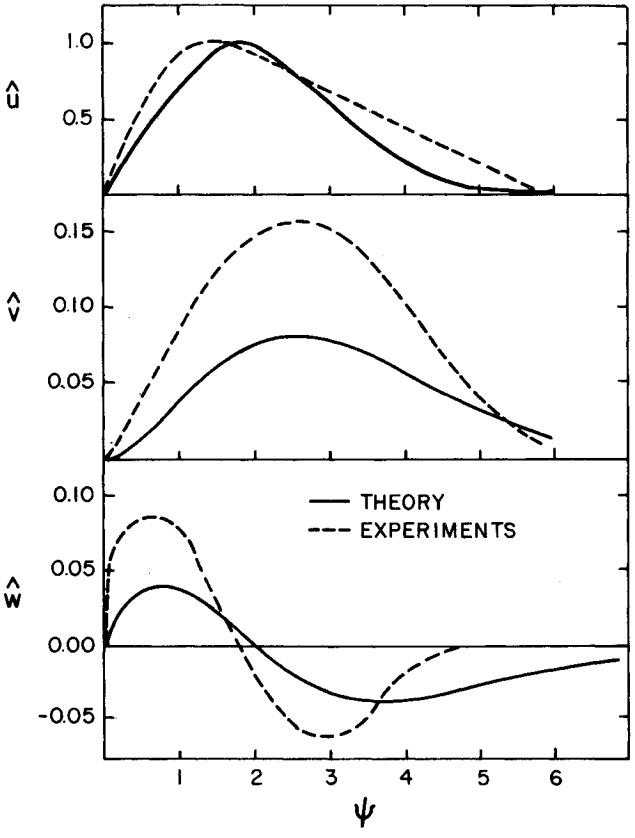

Fig. 7 Disturbance velocity field, comparison of theory with experiments (experimental data from Bippes[4] for $U_\infty=0.06$ m/s, $\Re=1$ m, $\lambda=1.7$ cm).

disturbance growth process. The growth process is well illustrated with the help of the local amplification rates as shown in Figs. 4 and 5. The experimental attempts to quantitatively measure the amplification rates are due to Tani[2] and Bippes.[4] Tani[2] measured disturbances occurring naturally in air flowing with velocity $U_\infty=11$ m/s over a wall of radius of curvature $\Re=10$ m. The observed disturbances correspond to the wavelength parameter $\Lambda=650$ and are marked with circles in Figs. 4 and 5. The measured amplification rate, $\beta=0.74$, agrees well with the theoretical value computed for the conditions described by the experimental point with the third lowest Görtler number (Fig. 4). However, since Tani[2] does not state which experimental point this value of the amplification rate is related to, we say only that the experimental and theoretical amplification rates are within the same range. Table 1 gives values of the amplification rates determined experimentally by Bippes,[4] who investigated the behavior of disturbances artificially forced into the boundary layer. The measured amplification rates are considerably smaller than their theoretical counterparts. However, as has been noted in Sec. III, these measurements were made with very strong disturbances and thus the nonlinear effects may be responsible for the slowing of the growth process.

Since the wavelength selection mechanism is determined by the disturbance growth process, one might presume that a vortex defined by the wavelength parameter Λ corresponding to the value that stays closest to the line of maximum amplification in Figs. 4 and 5 has the most favorable conditions to grow. It is known from experiments that the wavelength

Table 1 Comparison of observed and computed amplification rates at $U_\infty = 0.06$ m/s, $\mathcal{R} = 1$ m, and $\Lambda = 170$ (Ref. 4)

x, cm from leading edge	α	G	β experiments	β theory (ideal flow conditions)
27.5	0.742	5.92	0.933	2.27
37.5	0.861	7.4	1.126	3.11
47.5	0.966	8.8	1.340	4.09

selection mechanism acts only up to the establishment of the vortices, which are then preserved downstream regardless of the local growth rates. This points out the importance of the very initial stages of the instability process. The form of the curve of maximum amplification close to the neutral curve does not allow the choosing of the most dangerous vortex based only on the analysis of Figs. 4 and 5. However, if the vortices are not established until at least $G \simeq 2$ (and this is supported by the experimental data summarized in Figs. 4 and 5), then the vortices of $\Lambda \simeq 200$ should have the highest growth rates and should dominate the instability. The relative importance of different vortices can be checked by evaluating the total growth. The amplitude A^* of the disturbances changes according to

$$\frac{1}{A^*}\frac{dA^*}{d\phi^*} = \beta \tag{10}$$

where * denotes dimensional quantities. Then the total growth may be evaluated as

$$A^* = A_0^* \exp\left[\int_{\phi_0^*}^{\phi^*} \beta^* d\phi^*\right] \tag{11}$$

where $A_0^* = A^*(\phi_0^*)$. When dimensionless quantities are introduced, the above relations can be transformed to

$$A = \exp\left[\int_{G_0}^{G} \frac{4}{3}\frac{\beta}{G} dG\right] \tag{12}$$

where $A = A^*/A_0^*$ and $A(G_0) = 1$. Initial conditions corresponding to the neutral curve were adopted in all computations based on Eq. (12). It is convenient to introduce the amplification rate $\hat{\beta}$ defined as

$$\hat{\beta} = \beta/G \tag{13}$$

Since $\hat{\beta}$ appears explicitly in Eq. (12) describing the total growth of disturbances, $\hat{\beta}$ rather than β should be used to characterize the spatial amplification of the disturbances. This is the main reason for using $\hat{\beta}$ rather than β in Figs. 4 and 5. Additionally, the locus of maximum amplification points are more easily identified by using $\hat{\beta}$. The evaluation of the total growth has been carried up to $G = 20.0$, which corresponds to the downstream location where vortices are well developed, according to the experimental data (Figs. 4 and 5). One particular dimensional wavelength of the vortex ($\Lambda = \text{const}$) has been followed downstream for each integration. Figure 8 illustrates the distribution of the total growth for different vortices at streamwise locations corresponding to $G = 5.0$, 10.0, 15.0, and 20.0. The maxima of these curves define the most amplified and therefore the most dangerous disturbances. These maxima are located in the range of $\Lambda = (190, 210)$ regardless of the streamwise location. Bippes[4] noted that when the experimental apparatus did not favor any particular wavelength, the most amplified disturbances were observed. These corresponded to $\Lambda = 195$, 210, and 212 depending on the flow conditions. Thus, it appears that the theory compares well with the experiments. It should be mentioned that the maxima of the curves of the total amplification in Fig. 8, as well as minima of the curves of constant growth rate in Fig. 5, are relatively flat. Moreover, the growth rates for $G < 2.0$ are relatively small. Thus, a whole band of wavelengths may be equally predestined to emerge as a result of the instability and the good agreement between the theory and experiments may be coincidental. The experimental points due to Tani[2] and Tani and Sakagami[3] correspond to $\Lambda = 650$ and 1250 (Figs. 4 and 5). Total growths at $G = 20$ are given as exp(9.7) and exp(9.8), respectively, as compared with exp(11.65) for $\Lambda = 210$ (Fig. 8). These data suggest that under certain circumstances the wavelength selection mechanisms may be based on the maximum amplification rate of the initial disturbances. That is to say, the observed wavelength depends on the location (the value of G) of the initial conditions. Thus, the selection process may be very easily affected by the properties of the experimental apparatus that determine the entry location to the locus of the maximum amplification rate. Moreover, characteristics of the mean-flow disturbances can also affect wavelength selection.[4] The curves of the total growth as functions of the streamwise location are given in Fig. 9. These calculations correspond to the vortex wavelengths observed experimentally.[2-4] Note that the analysis of the behavior of the vortices under ideal flow conditions does not adequately explain the differences between these observations.

The neutral curve defines a location where the instability mechanism is activated. Disturbances become observable only at a certain distance downstream from this location, i.e., where their amplitudes become large enough to modify the mean-flow substantially. The minimum total growth that allows disturbances to become observable depends on the flow conditions. In all of the flow regimes studied by Tani and Sakagami,[3] $G = 2.0$ was the minimum value of the Görtler number at which vortices were observed. This corresponds to the total growth of vortices of $A = \exp(0.184)$. In the experiments by Bippes,[4] which compare well with the analysis of an ideal flow situation, disturbances had to grow by the factor of exp(1.68) to become observable at a Görtler number of $G = 5.62$. Thus, it may be possible to influence the wavelength selection process.

Under certain conditions, Görtler vortices may dominate the transition process. Experimental data related to transition are given by Liepmann[5,6] and Bippes.[4] The complexity of the process did not allow Bippes[4] to define the transition Görtler number. Liepmann[5,6] provided an estimate of the transition Görtler number to be $G = 16.6$ for the lowest level of turbulence in his wind tunnel. This estimate may be a little imprecise, but it allows us to extend the discussion. Let us assume that Liepmann[5,6] reproduced ideal flow conditions and thus transition in this experiment was caused by the most amplified disturbances. The disturbances grew by the factor of exp(8.93) from the location corresponding to the neutral curve. Note that an insignificant part of this growth (exp 1.68) occurred before disturbances became visible. However, this early growth is important because it is over this distance that the selection mechanism operates. The distance between the point of activation of the instability and the point of transition corresponds to an increase of Görtler number of about $\Delta G \simeq 16.1$. Part of this change, $\Delta G \simeq 5.1$, corresponds to the growth of disturbances before they are observable and part, $\Delta G \simeq 11$, corresponds to the growth after they are detected. Thus, the vortices are observable on the greater part of the distance between the point of activation of the instability and the transition location. Recall that the above discussion is based on the assumption that ideal flow conditions were generated experimentally. There are a number of possible departures from these conditions that

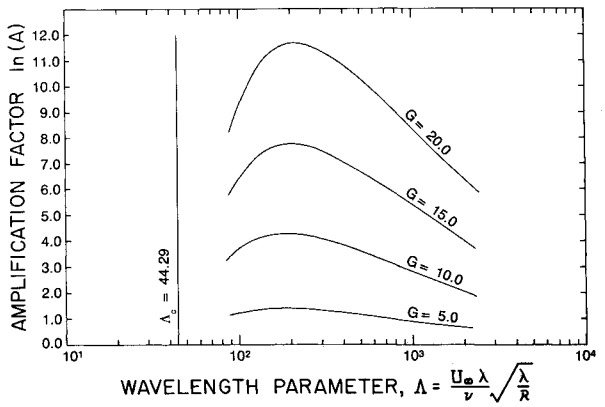

Fig. 8 Curves of total growth of disturbances as a function of the wavelength parameter Λ.

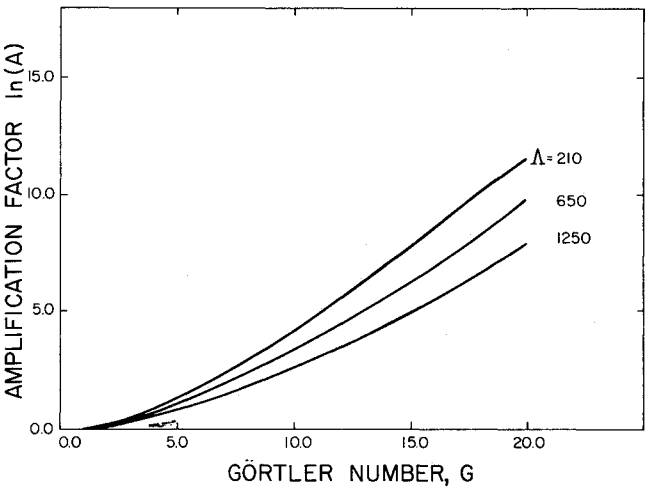

Fig. 9 Curves of total growth of disturbances as a function of Görtler number G for different values of the wavelength parameter Λ.

could have influenced experimental observation. Moreover, the definition of transition as caused by the Görtler vortices needs some clarification.

V. Effects of Mean-Flow Velocity

Bippes[4] observed that the manifestation of the Görtler vortices was strongly dependent on the nature of the mean-flow disturbance environment. This suggests that one possibility for a wavelength selection mechanism is the interaction of the streamwise vorticity of the mean-flow with the Görtler vortices.

Problem Formulation

The stability of a basic flow that consists of the superposition of the Blasius flow and a flow corresponding to counterrotating, streamwise vortex pairs is considered. Such vortices, whatever their source, once placed inside the boundary layer, are amplified or damped the same way as Görtler vortices.[1] The mean flow is described by

$$U = U_0(\phi_1,\psi) + \epsilon_s U_1(\phi_1,\psi)\cos\gamma z$$

$$V = \epsilon_v V_0(\phi_1,\psi) + \epsilon_s\epsilon_v V_1(\phi_1,\psi)\cos\gamma z$$

$$W = \epsilon_s\epsilon_v W_1(\phi_1,\psi)\sin\gamma z$$

$$P = \text{const} + \epsilon_s\epsilon_v^2 P_1(\phi_1,\psi)\cos\gamma z \qquad (14)$$

where subscript *0* refers to the Blasius flow and subscript *1* refers to the flow corresponding to the streamwise vortices. The parameter γ is a dimensionless spanwise wavenumber and ϵ_s a small dimensionless quantity indicating the strength of the streamwise vortices present in the mean flow. Definitions of the remaining symbols together with the proper scaling have been described in Sec. II. It should be noted that the u vortex velocity component is an order-of-magnitude larger than the v and w vortex velocity components. The small-disturbance quantities are superposed onto those given in Eq. (14) so that the total flow quantities become

$$U+\epsilon_p u'(\phi_1,\psi,z), \qquad V+\epsilon_p\epsilon_v v'(\phi_1,\psi,z)$$

$$W+\epsilon_p\epsilon_v w'(\phi_1,\psi,z), \qquad P+\epsilon_p\epsilon_v^2 p'(\phi_1,\psi,z) \qquad (15)$$

where ϵ_p is a small dimensionless quantity indicating the order of magnitude of the amplitude of the Görtler vortices. In this paper, ϵ_p is assumed to be much smaller than ϵ_s and ϵ_v so that terms of the order of ϵ_p^2 can be neglected when compared with $\epsilon_p\epsilon_s$ and $\epsilon_p\epsilon_v$. Substituting these total flow quantities into the field equations described by Floryan,[12] subtracting the basic-flow quantities, keeping the linear terms in the disturbance quantities, and then substituting Eq. (14), one obtains

$$T_1(U_0,V_0,u',v',w',p') = -\epsilon_s\left[\left(U_1\frac{\partial u'}{\partial\phi_1}+\frac{\partial U_1}{\partial\phi_1}u' + V_1\frac{\partial u'}{\partial\psi}+\frac{\partial U_1}{\partial\psi}v'\right)\cos\gamma z+\left(W_1\frac{\partial u'}{\partial z}-\gamma U_1 w'\right)\sin\gamma z\right] \qquad (16)$$

$$T_2(U_0,V_0,u',v',w',p') = -\epsilon_s\left[\left(U_1\frac{\partial v'}{\partial\phi_1}+\frac{\partial V_1}{\partial\phi_1}u' + V_1\frac{\partial v'}{\partial\psi}+\frac{\partial V_1}{\partial\phi_1}v'+2G^2U_1u'\right)\cos\gamma z + \left(W_1\frac{\partial v'}{\partial z}-\gamma V_1 w'\right)\sin\gamma z\right] \qquad (17)$$

$$T_3(U_0,V_0,u',v',w',p') = -\epsilon_s\left[\left(U_1\frac{\partial w'}{\partial\phi_1}+V_1\frac{\partial w'}{\partial\psi} + \gamma W_1 w'\right)\cos\gamma z+\left(\frac{\partial W_1}{\partial\phi_1}u'+\frac{\partial W_1}{\partial\psi}v'+W_1\frac{\partial w'}{\partial z}\right)\sin\gamma z\right] \qquad (18)$$

$$T_4(U_0,V_0,u',v',w',p') = 0 \qquad (19)$$

Operators T_1, T_2, T_3, and T_4 have been defined by Eqs. (4-7). Equations (16-19) need to be supplemented by initial and boundary conditions. The initial conditions are specified later, while the boundary conditions for an impermeable surface are the usual homogeneous conditions

$$u' = v' = w' = 0 \text{ at } \psi = 0$$

$$u', v', w' \to 0 \quad \text{as } \psi \to \infty \qquad (20)$$

The solution for the disturbances assumes the form

$$q'(\phi_1,\psi,z) = [\hat{q}_0(\psi,z)+\epsilon_s\hat{q}_1(\psi,z)]\exp[\int(\beta_0+\epsilon_s\beta_1)\,d\phi_1] \qquad (21)$$

where q' stands for any disturbance quantity. Substitution of Eq. (21) into Eqs. (16-20) and application of perturbation methods[15] results in the following:

1) Order ϵ_s^0

$$L_1(\hat{u}_0,\hat{v}_0,\hat{w}_0,\hat{p}_0)=\beta_0 U_0\hat{u}_0+\frac{\partial U_0}{\partial\phi_1}\hat{u}_0+V_0\frac{\partial\hat{u}_0}{\partial\psi}+\frac{\partial U_0}{\partial\psi}\hat{v}_0 - \frac{\partial^2\hat{u}_0}{\partial\psi^2}-\frac{\partial^2\hat{u}_0}{\partial z^2}=0 \tag{22}$$

$$L_2(\hat{u}_0,\hat{v}_0,\hat{w}_0,\hat{p}_0)=\beta_0 U_0\hat{v}_0+\frac{\partial V_0}{\partial\phi_1}\hat{u}_0+V_0\frac{\partial\hat{v}_0}{\partial\psi}+\frac{\partial V_0}{\partial\psi}\hat{v}_0 +2G^2U_0\hat{u}_0+\frac{\partial\hat{p}_0}{\partial\psi}-\frac{\partial^2\hat{v}_0}{\partial\psi^2}-\frac{\partial^2\hat{v}_0}{\partial z^2}=0 \tag{23}$$

$$L_3(\hat{u}_0,\hat{v}_0,\hat{w}_0,\hat{p}_0)=\beta_0 U_0\hat{w}_0+V_0\frac{\partial\hat{w}_0}{\partial\psi}+\frac{\partial\hat{p}_0}{\partial z} -\frac{\partial^2\hat{w}_0}{\partial\psi^2}-\frac{\partial^2\hat{w}_0}{\partial z^2}=0 \tag{24}$$

$$L_4(\hat{u}_0,\hat{v}_0,\hat{w}_0,\hat{p}_0)=\beta_0\hat{u}_0+\frac{\partial\hat{v}_0}{\partial\psi}+\frac{\partial\hat{w}_0}{\partial z}=0 \tag{25}$$

with homogeneous boundary conditions.

2) Order ϵ_s^1

$$L_1(\hat{u}_1,\hat{v}_1,\hat{w}_1,\hat{p}_1)=-\beta_1 U_0\hat{u}_0-\left(\beta_0 U_1\hat{u}_0+\frac{\partial U_1}{\partial\phi_1}\hat{u}_0 +V_1\frac{\partial\hat{u}_0}{\partial\psi}+\frac{\partial U_1}{\partial\psi}\hat{v}_0\right)\cos\gamma z-\left(W_1\frac{\partial\hat{u}_0}{\partial z}-\gamma U_1\hat{w}_0\right)\sin\gamma z \tag{26}$$

$$L_2(\hat{u}_1,\hat{v}_1,\hat{w}_1,\hat{p}_1)=-\beta_1 U_0\hat{v}_0-\left(\beta_0 U_1\hat{v}_0+\frac{\partial V_1}{\partial\phi_1}\hat{u}_0 +V_1\frac{\partial\hat{v}_0}{\partial\psi}+\frac{\partial V_1}{\partial\psi}\hat{v}_0+2G^2U_1\hat{u}_0\right)\cos\gamma z -\left(W_1\frac{\partial\hat{v}_0}{\partial z}-\gamma V_1\hat{w}_0\right)\sin\gamma z \tag{27}$$

$$L_3(\hat{u}_1,\hat{v}_1,\hat{w}_1,\hat{p}_1)=-\beta_1 U_0\hat{w}_0-\left(\beta_0 U_1\hat{w}_0+V_1\frac{\partial\hat{w}_0}{\partial\psi} +\gamma W_1\hat{w}_0\right)\cos\gamma z-\left(\frac{\partial W_1}{\partial\phi_1}\hat{u}_0+\frac{\partial W_1}{\partial\psi}\hat{v}_0+W_1\frac{\partial\hat{w}_0}{\partial z}\right)\sin\gamma z \tag{28}$$

$$L_4(\hat{u}_1,\hat{v}_1,\hat{w}_1,\hat{p}_1)=-\beta_1\hat{u}_0 \tag{29}$$

with homogeneous boundary conditions.

The initial conditions are taken such that the solution of the zeroth-order problem [Eqs. (22-25)] consists of a set of counterrotating vortices of spanwise wavenumber α,

$$[\hat{u}_0,\hat{v}_0,\hat{p}_0]=[u_0(\psi),v_0(\psi),p_0(\psi)]\cos(\alpha z)$$
$$\hat{w}_0=w_0(\psi)\sin\alpha z \tag{30}$$

Substitution of Eqs. (30) into Eqs. (22-25) yields the following eigenvalue problem:

$$\beta_0 U_0u_0+\frac{\partial U_0}{\partial\phi_1}u_0+V_0\frac{\mathrm{d}u_0}{\mathrm{d}\psi}+\frac{\partial U_0}{\partial\psi}v_0-\frac{\mathrm{d}^2u_0}{\mathrm{d}\psi^2}+\alpha^2u_0=0 \tag{31}$$

$$\beta_0 U_0v_0+\frac{\partial V_0}{\partial\phi_1}u_0+V_0\frac{\mathrm{d}v_0}{\mathrm{d}\psi}+\frac{\partial V_0}{\partial\psi}v_0+2G^2U_0u_0 +\frac{\mathrm{d}p_0}{\mathrm{d}\psi}-\frac{\mathrm{d}^2v_0}{\mathrm{d}\psi^2}+\alpha^2v_0=0 \tag{32}$$

$$\beta_0 U_0w_0+V_0\frac{\mathrm{d}w_0}{\mathrm{d}\psi}-\alpha p_0-\frac{\mathrm{d}^2w_0}{\mathrm{d}\psi^2}+\alpha^2w_0=0 \tag{33}$$

$$\beta_0u_0+\frac{\mathrm{d}v_0}{\mathrm{d}\psi}+\alpha w_0=0 \tag{34}$$

with homogeneous boundary conditions. The above equations define the Görtler stability problem for ideal flow conditions. One can solve Eqs. (31-34) for eigenvalues α, β, and G and obtain the respective eigenfunctions. The appropriate numerical procedure is described in Ref. 1.

Substituting Eqs. (30) into Eqs. (26-29) yields

$$L_1(\hat{u}_1,\hat{v}_1,\hat{w}_1,\hat{p}_1)=-\beta_1U_0u_0\cos\alpha z -\frac{1}{2}\left(\beta_0U_1u_0+\frac{\partial U_1}{\partial\phi_1}u_0+V_1\frac{\mathrm{d}u_0}{\mathrm{d}\psi}+\frac{\partial U_1}{\partial\psi}v_0\right)\cos(\gamma-\alpha)z +\frac{1}{2}(\alpha W_1u_0+\gamma U_1w_0)\cos(\gamma-\alpha)z+\text{N.S.T.} \tag{35}$$

$$L_2(\hat{u}_1,\hat{v}_1,\hat{w}_1,\hat{p}_1)=-\beta_1U_0v_0\cos\alpha z-\frac{1}{2}\left(\beta_0U_1v_0+\frac{\partial V_1}{\partial\phi_1}u_0 +V_1\frac{\mathrm{d}v_0}{\mathrm{d}\psi}+\frac{\partial V_1}{\partial\psi}v_0+2G^2U_1u_0\right)\cos(\gamma-\alpha)z +\frac{1}{2}(\alpha W_1v_0+\gamma V_1w_0)\cos(\gamma-\alpha)z+\text{N.S.T.} \tag{36}$$

$$L_3(\hat{u}_1,\hat{v}_1,\hat{w}_1,\hat{p}_1)=-\beta_1U_0w_0\sin\alpha z-\frac{1}{2}\left(\beta_0U_1w_0+V_1\frac{\mathrm{d}w_0}{\mathrm{d}\psi} +\gamma W_1w_0\right)\sin(\gamma-\alpha)z-\frac{1}{2}\left(\frac{\partial W_1}{\partial\phi_1}u_0+\frac{\partial W_1}{\partial\psi}v_0+\alpha W_1w_0\right) \times\sin(\gamma-\alpha)z+\text{N.S.T.} \tag{37}$$

$$L_4(\hat{u}_1,\hat{v}_1,\hat{w}_1,\hat{p}_1)=-\beta_1u_0\cos\alpha z \tag{38}$$

with homogeneous boundary conditions and where N.S.T. stands for terms that are proportional to $\cos(\gamma+\alpha)z$ or $\sin(\gamma+\alpha)z$ that do not produce secular terms in $\hat{u}_1$, $\hat{v}_1$, $\hat{w}_1$, or $\hat{p}_1$.

Since the homogeneous parts of Eqs. (35-38) are the same as Eqs. (31-34) and since the latter have a nontrivial solution, the inhomogeneous Eqs. (35-39) have a solution if and only if the inhomogeneous parts are orthogonal to every solution of the adjoint homogeneous problem.[15] These solvability conditions depend on whether $\gamma=2\alpha$ or not. If γ is away from 2α, satisfying the solvability conditions requires setting $\beta_1=0$ and thus the Görtler vortices are unaffected by the presence of the vorticity in the mean flow. If $\gamma=2\alpha$, the correction for the amplification rate is given as

$$\beta_1=g_1/g_2 \tag{39}$$

where

$$g_1 = \frac{1}{2}\int_0^\infty \Big[\Big(-\beta_0 U_1 u_0 - \frac{\partial U_1}{\partial \phi_1} u_0 - V_1 \frac{du_0}{d\psi} - \frac{\partial U_1}{\partial \psi} v_0 + \alpha W_1 u_0 + \gamma U_1 w_0\Big)\zeta_1 + \Big(-\beta_0 U_1 v_0 - \frac{\partial V_1}{\partial \phi_1} u_0 - V_1 \frac{dv_0}{d\psi} - \frac{\partial V_1}{\partial \psi} v_0 - 2G^2 U_1 u_0 + \gamma W_1 v_0 + \gamma V_1 w_0\Big)\zeta_2 + \Big(\beta_0 U_1 w_0 - V_1 \frac{dw_0}{d\psi} + \gamma W_1 w_0 - \frac{\partial W_1}{\partial \phi_1} u_0 - \frac{\partial W_1}{\partial \psi} v_0 - \alpha W_1 w_0\Big)\zeta_3\Big] d\psi \quad (40)$$

$$g_2 = \int_0^\infty (U_0 u_0 \zeta_1 + U_0 v_0 \zeta_2 + U_0 w_0 \zeta_3 + u_0 \zeta_4)\, d\psi \quad (41)$$

and ζ_1, ζ_2, ζ_3, and ζ_4 are solutions of the adjoint homogeneous problem.

The mean-flow vortex components appearing in Eqs. (40) and (41) are amplified the same way as Görtler vortices.[1] Thus, they assume the form

$$[U_1, V_1, P_1] = [U_1(\psi), V_1(\psi), P_1(\psi)]\exp(\int \sigma d\phi_1)$$
$$W_1 = W_1(\psi)\exp(\int \sigma d\phi_1) \quad (42)$$

where σ is the amplification rate of the mean-flow vorticity. Substitution of Eq. (42) into Eq. (40) results in

$$g_1 = \tfrac{1}{2} F \exp(\int \sigma d\phi_1) \quad (43)$$

where the expression for F can be easily deduced. Equation (43) suggests a very strong interaction effect. The amplification rate correction β_1 grows exponentially like the mean-flow vortex. Thus, the growth of the disturbance due to the interaction will be double exponential and may quickly dominate the instability process.

The double exponential growth appears to be typical of problems of this type, as shown by Nayfeh[13] for vortices affecting Tollmien-Schlichting waves and Herbert and Morkovin[14] for Tollmien-Schlichting waves affecting Görtler vortices. In the case considered here, any latent streamwise vorticity can strongly influence the observation of the spanwise wavelength by amplifying a narrow band of wavelengths. In some sense, this is related to the experimental technique of strongly fixing the spanwise wavelength by either introducing mean-flow vorticity[7] or changing the spanwise boundary conditions.[4]

Numerical Results and Discussion

The amplification rate correction β_1 has to be evaluated numerically and the appropriate numerical procedure is described in Ref. 16.

Equations (39-41) defining β_1 are valid when the mean-flow vorticity constitutes only a small fraction of the basic flow. Since the correction β_1 grows exponentially in the streamwise direction [see Eqs. (39-42)], its value may be interpreted only locally. It is then sufficient to evaluate

$$\tilde{\beta}_1 = \beta_1 / \exp(\int \sigma d\phi_1) \quad (44)$$

The above definition of the correction $\tilde{\beta}_1$ does not include effects of the variations of the mean-flow vorticity from one chordwise location to another. The value of $\tilde{\beta}_1$ depends directly on the way the solution of the mean-flow vorticity is normalized. For the present calculations, the normalization was chosen in such a way that $\max u_1 = 1$. Then, the parameter ϵ_s introduced in Eq. (14) may be interpreted as defining the relative strength of the mean-flow vorticity as compared to the Blasius boundary layer.

The numerical computations were performed for the three values of the wavelength parameter Λ corresponding to the experimental observations by Tani and Sakagami[3] ($\Lambda = 650$, 1250) and Bippes[4] ($\Lambda = 210$). The disturbances were allowed to interact with the resonant wavelength from the mean-flow vorticity. The results are presented in Table 2.

Tani and Sakagami[3] observed disturbances naturally occurring in their experimental apparatus. They concluded that the vortex wavelength depended on the particular properties of the experimental apparatus and that the wavelength they observed did not correspond to the most amplified disturbance. This agrees qualitatively with the results presented in Table 2. For the Görtler numbers close to the neutral curve, i.e., where the wavelength selection mechanism is active, effects of the interaction tend to accelerate growth of the vortices. Thus, it is possible that the mean-flow in the experimental apparatus used by Tani and Sakagami[3] contained vorticity that gave rise to the disturbances corresponding to $\Lambda = 650$ and 1250.

Bippes[4] investigated the effects of the mean-flow disturbances on the naturally occurring Görtler vortices and concluded that the wavelength selection mechanism is influenced by the particular form of the oncoming disturbances. When all possible disturbances were introduced into the oncoming flow, the Görtler vortices corresponding to the most amplified wavenumber ($\Lambda = 210$) were observed. For small values of Görtler number, the corrections to the amplification rate $\tilde{\beta}$, corresponding to vortices characterized by $\Lambda = 210$, are larger than for vortices characterized by $\Lambda = 650$ and 1250 (Table 2). This might suggest that the interaction mechanism is strongest for the most amplified vortices. However, this supposition has been checked and was found not to be true. Therefore, it may be concluded that when an isotropic field of disturbances is present in the oncoming flow, the interactions between the vortices and mean-flow vorticity do not affect the wavelength selection mechanism.

Bippes[4] also investigated the streamwise vortices that were artificially forced into the boundary layer. He measured the amplitudes and calculated the amplification rates. His data are presented in Table 1. Note that the experimental amplification rates for high Görtler numbers are much smaller than their theoretical counterparts. This lower amplification

Table 2 Amplification rate correction $\tilde{\beta}_1$ [Eq. (44)] due to the interaction of disturbances with the mean-flow vorticity

G	$\Lambda = 210$	$\Lambda = 650$	$\Lambda = 1250$
1.0	0.465	0.244	0.185
1.5	0.505	0.260	0.215
2.0	0.450	0.195	0.180
2.5	0.338	0.074	0.097
3.0	0.189	−0.088	−0.023
3.5	0.011	−0.282	−0.174
4.0	−0.189	−0.500	−0.348
4.5	−0.409	−0.739	−0.541
5.0	−0.646	−0.995	−0.751
5.5	−0.899	−1.269	−0.974
6.0	−1.167	−1.555	−1.211
6.5	−1.447	−1.854	−1.456
7.0	−1.740	−2.168	−1.712
7.5	−2.048	−2.499	−1.979
8.0	−2.368	−2.833	−2.254
8.5	−2.694	−3.180	−2.534
9.0	−3.031	−3.540	−2.825
9.5	−3.379	−3.916	−3.125
10.0	−3.737	−4.305	−3.436

rate was attributed to some type of interaction between disturbances, since the observed amplitudes were quite large (see Sec. IV). The model presented here may be interpreted as describing the interaction between two sets of Görtler vortices. The results presented in Table 2 show that the vortex-vortex interaction lowers the amplification rate for Görtler numbers greater than 3, which is in qualitative agreement with the experimental observations summarized in Table 1.

VI. Conclusions

An analysis of the wavelength selection mechanism and growth of Görtler vortices is presented. Results show that under ideal flow conditions the most amplified disturbances will result from the basic instability process. The wavelength selection mechanism and the disturbance growth process are easily affected by departures from ideal flow conditions. When mean-flow vorticity is considered, the growth of disturbances due to the interaction is double exponential and may quickly dominate the instability process. Numerical results show that in the region close to the neutral curve, where the wavelength selection process is under way, streamwise vorticity of the spanwise wavenumber γ excites disturbances of the wavenumber $\gamma/2$ and therefore these disturbances, rather than the most amplified ones, may result from the instability. Far downstream from the location corresponding to the neutral curve, where vortices are well developed, the interaction process tends to slow the growth of the disturbances.

Acknowledgments

This work was supported by NASA Langley Research Center under Grant NSG-1255 and a grant from the Natural Sciences and Engineering Research Council of Canada.

References

[1]Floryan, J. M. and Saric, W. S., "Stability of Görtler Vortices in Boundary Layers," *AIAA Journal*, Vol. 20, March 1982, pp. 316-324.

[2]Tani, I., "Production of Longitudinal Vortices in the Boundary Layer along a Curved Wall," *Journal of Geophysical Research*, Vol. 67, No. 8, 1962, pp. 3075-3080.

[3]Tani, I. and Sakagami, J., "Boundary Layer Instability at Subsonic Speeds," *Proceedings of Third Congress of the International Council of Aerospace Sciences*, Stockholm, 1962, Spartan, Washington, D.C., 1964, pp. 391-403.

[4]Bippes, H., "Experimentelle Untersuchung des laminar-turbulenten Umschlags an einer parallel angeströmten konkaven Wand," Sitzungsberichte der Heidelberger Akademie der Wissenschaften Mathematischnaturwissenschaftliche Klasse, 3 Abhandlund, Jahrgang 1972, pp. 103-180 (also NASA TM-72243, March 1978).

[5]Liepmann, H. W., "Investigations of Laminar Boundary Layer Stability and Transition on Curved Boundaries," NACA Wartime Rept. W-107, 1943.

[6]Liepmann, H. W., "Investigations on Boundary Layer Transition on Concave Walls," NACA Wartime Rept. W-87, 1945.

[7]Wortmann, F. X., "Experimentelle Untersuchungen laminarer Grenzschichten bei instabilier Schichtung," *Proceedings of XI International Congress on Applied Mechanics*, Munich, edited by H. Görtler, Springer-Verlag, Berlin, 1964, pp. 815-825.

[8]Wortmann, F. X., "Experimental Investigations of Vortex Occurrence at Transition in Unstable Laminar Boundary Layers," AFOSR Rept. 64-1280, AF 61 (052)-220, 1964.

[9]Wortmann, F. X., "Visualization of Transition," *Journal of Fluid Mechanics*, Vol. 38, 1969, pp. 473-480.

[10]Smith, A. M. O., "On the Growth of Taylor-Görtler Vortices Along Highly Concave Walls," *Quarterly Journal of Applied Mathematics*, Vol. 13, No. 3, 1955, pp. 233-262 (also Douglas Aircraft Rept. ES-17110, 1953).

[11]Herbert, Th., "Higher Eigenstates of Görtler Vortices," *Theoretical and Experimental Fluid Mechanics*, edited by U. Müller, K. B. Roesner, and B. Schmidt, Springer-Verlag, New York, 1979, pp. 322-330.

[12]Floryan, J. M., "Stability of Boundary-Layer Flows over Curved Walls," Ph.D. Thesis, Virginia Polytechnic Institute and State University, Blacksburg, Jan. 1980.

[13]Nayfeh, A. H., "Effects of Streamwise Vortices on Tollmien-Schlichting Waves," *Journal of Fluid Mechanics*, Vol. 107, 1981, pp. 441-453.

[14]Herbert, Th. and Morkovin, M. V., "Dialogue on Bridging Some Gaps in Stability and Transition Research," *IUTAM Symposium on Laminar-Turbulent Transition*, Stuttgart, FRG, Springer-Verlag, 1980, pp. 47-72.

[15]Nayfeh, A. H., *Introduction to Perturbation Techniques*, Wiley-Interscience, New York, 1981.

[16]Floryan, J. M. and Saric, W. S., "Wavelength Selection and Growth of Görtler Vortices," AIAA Paper 80-1376, July 1980.